Author's draft of the accepted paper for IET Microwaves, Antennas & Propagation, May 2019

Design of multi-standard single/tri/quint-wideband asymmetric stepped-impedance resonator filters with adjustable TZs

Yasir I. A. Al-Yasir[1], Yuxiang Tu[1], Mustafa. S. Bakr[2], Naser Ojaroudi Parchin[1], A. Asharaa[1], W. A. Mshwat[1], Raed A. Abd-Alhameed[1,*], James M. Noras[1]

[1]School of Electrical Engineering & Computer Science, Bradford University, Bradford, UK
[2]Institute of Microwave and Photonics, University of Leeds, Leeds, UK.
[*]r.a.a.abd@bradford.ac.uk

Abstract: This paper presents an original Asymmetric Stepped-Impedance Resonator (ASIR) filter combined with meander coupled-line structures and enabling the realisation of finite transmission zeros and the implementation of multi-band bandpass filters. The meander coupled sections tune the transmission zeros and resonant frequencies: with higher order spurious frequencies cancelled by the transmission zeros, a single wide band with wide stopband from 1.18 to 1.84 GHz is possible. Furthermore, by positioning the finite transmission zeros between the high order spurious frequencies and adjusting the coupling strength between resonators, a quint-wideband filter can be realized, with centre frequencies of 1.19, 4.29, 5.43, 6.97, 9.9 GHz and fractional bandwidths of 31.9%, 15.4%, 15.8%, 4.3%, 39.2% respectively. More importantly, two filters with single-/quad-wideband performance can be realized by tuning the parameters of the meander coupled section and therefore they can be designed separately by using only one original structure. The triple-wideband filter is realized with the help of the asymmetric parallel uncoupled microstrip section. These filter structures enjoy the advantage of single-/multi-band versatility, structure reusability and simplicity. The good in-band and out-of-band performance, low loss, and simple structure of the proposed single/tri/quint-wideband filters make them very promising for applications in future multi-standard wireless communication.

1. Introduction

With the growth of multi-service wireless communication networks, microwave components and systems that support various modern communication standards have become increasingly important. In particular, multi-standard bandpass filter (BPF) design demands high performance with compact size for enhanced system functionality. Such filters are usually required to be capable of covering the operating bands of the Global Positioning System (GPS: 1227.6 MHz, 1.57 GHz), System for Mobile Communication (GSM: 1800/1900 MHz etc.), the Universal Mobile Telecommunications System (UMTS: 1710-1880/1850-1990/1920-2170 MHz etc.) and IEEE 802.11a (5 GHz). Suitable filters need to have relative high fractional bandwidth, low insertion loss and low return loss. However, the need for filters to be physically small means that many designs are inadequate, failing to cover the required frequency bands due to their narrow bandwidth and low fractional bandwidth [1-5]. Increasing the size or requiring extra structures, such as via holes, means that the resulting filters are too complicated for fabrication and are difficult to integrate within multi-standard wireless communication systems [6-10, 12-17]. Critically, most proposed filter structures [1, 18] can only realize single band or multi-band performance by utilizing various different structures, which results in lower reusability, higher complexity and higher cost. Compared to the traditional stepped impedance resonator (SIR) with two step discontinuities, the asymmetric SIR (ASIR) has only one discontinuity but retains controllability of spurious modes. Thus, it combines the advantages of compact size, lower loss, and strong design feasibility, particularly in high-order BPFs such as dual band [18], triple band and quad band [22], because of its inherent higher order resonant modes. Published coupled line ASIR structures can be classified into two types: anti-parallel-coupled or parallel-coupled ASIRs. The Anti-Parallel-Coupled ASIR (APC-ASIR), consisting of two ASIR units with their high and/or low impedance lines anti-coupled with each other, is usually folded at its open end. In [18], the high impedance lines of two ASIRs are bent and coupled with each other to form a signal transmission route, and the first spurious frequency is utilized to form the second operating band [19]. Because the frequency response characteristic of the anti-parallel-coupled line is determined by the frequency response characteristic of the ASIR, the APC-ASIR frequency response is easy to calculate. However, the bandwidth characteristic of the APC-ASIR structure [18, 20], as with the multi-stage coupled ASIR structure [21, 22], is usually limited within the narrow band characteristic range and is not suitable to realize wide band performance. Therefore, this approach cannot fully meet the multi-service requirement of current wireless communication.

The second type, the parallel-coupled ASIR structure, has ASIRs with their high impedance lines parallel coupled with each other: this is also called the skew-symmetrical ASIR (SS-ASIR) coupled pair. Using this kind of structure, characteristics of frequency response performance such as bandwidth, return loss and insertion loss can be greatly improved at some frequency points, without changing or degrading the performance generally. This facilitates designs with wide bandwidth and large fractional bandwidth, different from the narrow band characteristic exhibited in traditional ASIR structures [18 - 20]. However, until now, the proposed ASIR structures could only realize narrow band characteristics [18 - 22] or dual/quad-wideband characteristics, with the disadvantages of uncontrollable or limited transmission zeros seriously restricting their application range.

In this work, we propose novel multi-standard single/tri/quint-wideband ASIR filters to solve the problems mentioned above. The proposed filters are capable of generating wide operating bands which effectively cover the GPS/GSM/UMTS/IEEE 802.11a application in wireless communication systems, including the GPS (1227 MHz, 1.57 GHZ), the GSM1800/1900 (1710-1880 MHz, 1850–1990 MHz), and the UMTS (1920–2170 MHz). These filters share the same original structure, with their performance optimized by tuning relative transmission zeros. Therefore, the design enjoys advantages of versatility and simplicity, with reduced design complexity and cost. Good agreement is observed between the simulated and measured results. Although a slight difference at the higher frequencies can be observed, this mismatch can be explained by an error in the manufacturing process or/and a variation in the material properties. In fact, the fabrication tolerances, as well as the SMA connectors and the calibration errors, may have led to the discrepancies between the simulated and measured results in the upper stopband.

To the best of the authors' knowledge, the proposed ASIR filters realize for the first time a single wideband filter with wide stop band and a quint-wideband filter at the same time, by using the same structure as in recently proposed single/multi-band filters [1 - 22]. Moreover, a quint-wideband filter can be realised with large fractional bandwidths for all operating bands in comparison with [12 - 14].

The proposed filters use the capacitive coupling of only two miniaturized ASIRs to realize single/tri/quint-wideband operation without adding any extra structure such as via holes or defected ground structure, which is also novel for single/multi-wideband filters [1 - 22].

2. The In-Band Performance Enhancement Method and Transmission Zeros Adjusting Method

2.1 The In-band Performance Enhancement Method

To enhance the filter in-band performance, the SS-ASIR structure is used. In the design, the frequency response transformation relationship between the parallel-coupled ASIR and the ASIR unit needs to be considered so as to enhance the performance in the desired frequency band. In Fig. 1, the electrical length ratio α equals $\theta_2/(\theta_2+\theta_1)$, where θ_1 and θ_2 are the electrical lengths of section L_2 and L_1 in the ASIR, respectively. The characteristic impedance ratio K equals Z_2/Z_1, where Z_1 and Z_2 is the characteristic impedance of section L_2 and L_1 in the ASIR, respectively. The transformation relationship table is shown in Table 1.

Fig. 1. *Structure of an asymmetric SIR*

2.2 The Transmission Zeros Generating and Tuning Method in the SS-ASIR structure

Fig. 2 (a) shows the topological structure of the SS-ASIR coupled pair rearranged by the meander coupled lines (MCL) to form the (SSMCL-ASIR), which is shown as the grey part with width W_3 and length L_4, respectively. The meander coupled section is added at the open end of the high impedance coupled line in the SS-ASIR coupled pair. Fig. 2 (b) shows the equivalent circuit and the coupling routing scheme of Fig. 2 (a).

Table 1 The transformation relationship of in-band performance of the SS-ASIR coupled pair and ASIR unit, when α ranges from 0.4 to 0.7

α	Funda-mental Frequency f_0	First spurious Frequency fs1	Second spurious Frequency fs2	Third Spurious Frequency fs3	Fourth Spurious Frequency fs4
0.4	Improved	NC/DE	Improved	NC/DE	Improved
0.42	Improved	NC/DE	Improved	NC/DE	Improved
0.5	Improved	NC/DE	Improved	NC/DE	Improved
0.55	Improved	NC/DE	NC/DE	Improved	NC/DE
0.57	Improved	NC/DE	Improved	Improved	NC/DE
0.6	Improved	Improved	NC/DE	Improved	NC/DE
0.65	Improved	Improved	NC/DE	NC/DE	Improved
0.7	Improved	Improved	NC/DE	NC/DE	NC/DE

''Improved'' means significantly enhanced performance at relative frequency; ''NC/DE'' means no significant change or degradation of performance at relative frequency point.

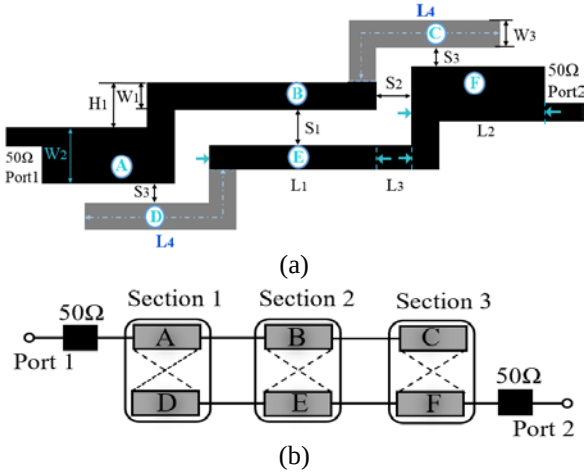

Fig. 2. *A SS-ASIR coupled pair with meander coupled section.* ***(a)*** *The schematic diagram.* ***(b)*** *Equivalent circuit and coupling routing scheme for the proposed filter.*

The main signal is coupled to the two half-wavelength resonators at the same time, providing the two main paths between the two ports. Each ASIR resonator of the filter consists of three cascaded sections. The A-B-C sections form the first resonator (ASIR1) and D-E-F sections form the second resonator (ASIR 2). In addition to the usual single coupling route of B-E for the main coupled transmission lines represented by section 2, two extra coupling routes, namely A-D for section 1 and C-F for section 3, are created by the adoption of meander coupled lines. This multi-path coupling routing scheme of the modified SSMCL-ASIR filter is shown in Fig. 2 (b). Due to the multi-path coupling routing, more transmission zeros (TZs) are created, which are utilized to suppress high order spurious frequencies or to help facilitate multi-band performance.

Because the harmonic frequency performance would degrade when using the SS-ASIR structure, first spurious Frequency (f_{si}) cannot be conveniently deduced by simply analysing $Y_{in} = 0$ in the ASIR unit. However, transmission zero frequency (f_{zi}) can still be obtained by setting $Z_{ine} = Z_{ino}$, where Z_{ine} and Z_{ino} are the input impedances for the even- or odd-mode equivalent circuits, respectively. The necessary and sufficient conditions for $Z_{ine} = Z_{ino}$ is $S_{21} = 0$ and the equivalent Y-parameter matrix of the even or odd mode

equivalent circuit of the proposed structure can be expressed as:

$$\begin{bmatrix} y_{21} & y_{22} \end{bmatrix} = \begin{bmatrix} j\frac{Z_{0even}-Z_{0odd}}{2}\csc(\theta_{01}+\theta_4) & -j\frac{Z_{0even}+Z_{0odd}}{2}\cot(\theta_{01}+\theta_4) \end{bmatrix}$$

$$B = -Z_{0even}Z_{0odd}\cot^2(\theta_{01}+\theta_4) + \frac{(Z_{0even}-Z_{0odd})^2}{4} \quad (1)$$

where θ_{01} and θ_4 are the electrical lengths of the original coupled line and of the meander coupled section, respectively. Z_{0even} and Z_{0odd} are the even and odd mode characteristic impedances for each coupled section, respectively.

Since all elements of the normalized Y-parameters in (1) are purely imaginary, S_{21} of this coupled line can be expressed as:

$$S_{21} = -\frac{2j\,\mathrm{Im}\{y_{12}\}}{1-\mathrm{Im}\{y_{11}\}^2+\mathrm{Im}\{y_{12}\}^2+2j\,\mathrm{Im}\{y_{11}\}} \quad (2)$$

Substituting from (1) into (2), gives equation (3) (see (3)). According to equation (3), there are three cases leading to $S_{21} = 0$. The first case is $Z_{0even} = Z_{0odd}$. The meander coupled section of length L_4 can be seen as a shifted coupled line structure which can suppress the spurious peak by compensating even-mode and odd-mode phase velocities. When the coupled line insertion loss is zero, the coupled length for the shifted coupled line/meander coupled line can be obtained from the following:

$$\frac{Z_{0even}}{Z_{0odd}} = \frac{\sin\beta_{even}L_4}{\sin\beta_{odd}L_4} \quad (4)$$

when $Z_{0even} = Z_{0odd}$, $\sin\beta_{even}L_4 = \sin\beta_{odd}L_4$. Also,

$$\beta_{even}L_4 = \beta_{odd}L_4 + k_1\pi \qquad (k_1 = 0,1,2,3...) \quad (5)$$

In this design, $0<\beta_{even}L_4<\pi$ and $0<\beta_{odd}L_4<\pi$, thus $k_1 = 0$ and $\beta_{even} = \beta_{odd}$. Because $v_{p,even} = \omega_{even}/\beta_{even}$ and $v_{p,odd} = \omega_{odd}/\beta_{odd}$, then $v_{p,\,even} = v_{p,odd}$ when $\omega_{even} = \omega_{odd}$. $v_{p,even}$, ω_{even} and β_{even} are even-mode phase velocity, angular frequency and phase constant, respectively. $v_{p,odd}$, ω_{odd} and β_{odd} mean odd-mode phase velocity, angular frequency and phase constant, respectively. When the even-mode and odd-mode phase velocities are equal, transmission zeros are generated and the spurious peak can be suppressed. Fig. 3 compares frequency responses with and without a shifted coupled line/meander coupled section (SCL/MCS). As shown in the figure, without a SCL/MCS the unsuppressed spurious frequencies fs2 and fs3 exist and seriously limit the stop band bandwidth. With a SCL/MCS, fs2 and fs3 are effectively suppressed and a wide stop band is generated. Moreover, because the whole coupled line length is extended by the SCL/MCS structure, both the fundamental and spurious frequencies are shifted to lower frequencies.

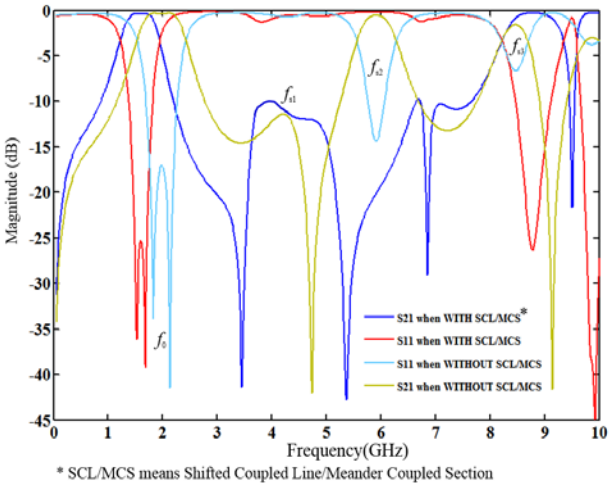

Fig. 3. *Frequency response comparison with and without SCL/MCS.*

$$\begin{aligned} &4-(Z_{0even}+Z_{0odd})^2\cdot\frac{\cos^2(\theta_{01}+\theta_4)}{\sin^2(\theta_{01}+\theta_4)}+(Z_{0even}-Z_{0odd})^2\cdot\frac{1}{\sin^2(\theta_{01}+\theta_4)}+4j(Z_{0even}+Z_{0odd})\cdot\frac{\cos(\theta_{01}+\theta_4)}{\sin(\theta_{01}+\theta_4)} \\ &=-\frac{4j(Z_{0even}-Z_{0odd})\cdot\sin(\theta_{01}+\theta_4)}{u+jv} \\ &=\frac{4j(Z_{0even}-Z_{0odd})\cdot\sin(\theta_{01}+\theta_4)}{v^2-u^2}\cdot(u+jv) \end{aligned} \quad (3)$$

where,

$$\begin{cases} u = 4\sin^2(\theta_{01}+\theta_4)-(Z_{0even}+Z_{0odd})^2\cdot\cos^2(\theta_{01}+\theta_4)+(Z_{0even}-Z_{0odd})^2 \\ v = 4(Z_{0even}+Z_{0odd})\cdot\cos(\theta_{01}+\theta_4)\sin(\theta_{01}+\theta_4) \end{cases}$$

The second case is sin ($\theta_{01}+\theta_4$) = 0, namely

$$\theta_{01}+\theta_4 = k\pi \quad (k=1, 2, 3\ldots). \tag{6}$$

When k = 1 for the shortest whole coupled line electrical length, $\theta_{01}+\theta_4 = \pi$, and the corresponding coupled line physical length can be calculated as:

$$L_1+L_4 = \frac{\lambda_g}{2} \tag{7}$$

where, L_1 and L_4 are the physical lengths corresponding to θ_{01} and θ_4, respectively. The third case is u=0 and v=0. When u=0:

$$\theta_{01}+\theta_4 = 2\sin^{-1}\sqrt{\frac{Z_{0even}Z_{0odd}}{(Z_{0even}+Z_{0odd})^2+4}} \tag{8}$$

Equation (8) shows the relationship between the whole coupled line electrical length and odd-mode and even-mode impedance of the whole coupled lines. When v=0, sin $[2(\theta_{01}+\theta_4)] = 0$:

$$\theta_{01}+\theta_4 = \frac{k\pi}{2} \quad (k=1, 2, 3\ldots). \tag{9}$$

In general, the shortest whole coupled line electrical length to realize $S_{21} = 0$ can be got in the third case when k is equal to 1 and $\theta_{01}+\theta_4 = \pi/2$. The corresponding coupled line physical length can then be calculated as:

$$L_1+L_4 = \frac{\lambda_g}{4} \tag{10}$$

3. The Single-Wideband ASIR Filter Design

According to the frequency response transformation relationship discussed in Section 2, the electrical length ratio α is 0.57 when L_2 is 11.4 mm, thus setting the fundamental frequency to around 1.51 GHz. The in-band performance of the first band, such as the insertion loss and return loss, is improved when the impedance ratio K is 0.48.

The dimensions of the resonator are chosen as follows: L_1 = 14 mm, L_2 = 11.4 mm, L_1+L_3 = 15.2 mm, W_1 = 0.4 mm and W_2 = 1.6 mm. Through the design procedure for the coupled resonator circuits, the gaps of the whole coupled lines in Fig. 2 are determined as S_1 = 1.2 mm, S_2 = 0.2 mm and S_3 = 0.4 mm. The use of different gaps adds more design freedom for the filter. For simplicity of design, the meander coupled structure width W_3 is made 0.4 mm, which is the same as the width of coupled lines.

Because the fundamental frequency is 1.51 GHz, the relative λ_g can be calculated as 77.4 mm. Therefore, the value of (L_1+L_4) is about 19.4 mm. L_1 is 14 mm, so L_4 is set at around 5.4 mm. Although sections L_3 and H_1 would become coupled parts after adding the meander coupled section, the effects are small. The influence of these sections to the overall performance can therefore be disregarded, their coupling being much weaker than that involving sections L_1 and section L_4.

To further analyse the influence of the meander coupled section on the resonance frequency fsm and transmission zero frequencies fzn, the normalized fsm (m = 1, 2, 3, 4) and normalized fzn (n = 1, 2, 3, 4) versus γ for different values of K, are illustrated in Fig. 4, where γ is the electrical length ratio between the meander coupled section θ_4 and whole coupled line ($\theta_1+\theta_4$) and $\gamma = \theta_4/(\theta_1+\theta_4)$.

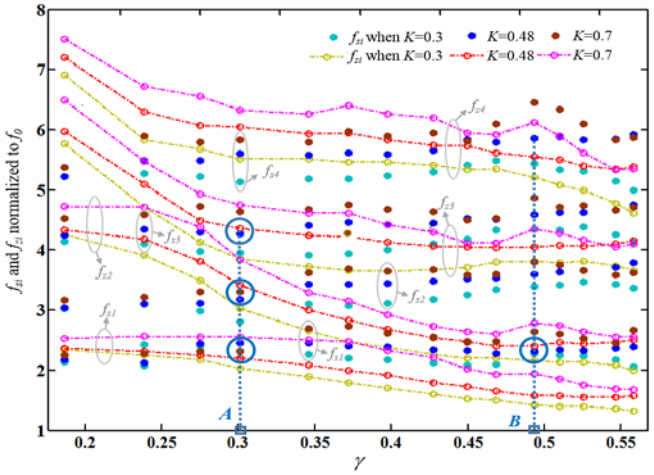

Fig. 4. *fsi and fzi normalized to f0 versus γ for different values of K in SSMCL-ASIR structure.*

It can be seen in Fig. 4 that for a fixed K value, the normalized fzn (n = 1, 2, 3, 4) decline continuously and the normalized fsm (m = 1, 2, 3, 4) follow an approximate sinusoidal curve when γ ranges from 0.17 to 0.58. Larger K values result in larger normalized fzi and larger normalized fsi for a fixed γ value. Because the normalized fsi follow an approximate sinusoidal curve and fzi follow a decreasing curve, they can intersect at a certain γ value. As illustrated, at point A, when K = 0.30, fz1 approaches fs1, fz2 approaches fs2 and fz3 approaches fs3, respectively. That means the first spurious frequency, the second spurious frequency and the third spurious frequency are suppressed successfully when K = 0.30. The corresponding L_4 can be calculated as 5.7 mm, which is close to the theoretical value.

The coupling matrix discussed in reference [23] will not be discussed in this paper because of its wideband limitation [23-24]. The coupling between two ASIRs can be represented by a J-inverter susceptance $J_{1,2}$, where subscript 1 and 2 denotes the first and second passband. A larger value of $J_{1,2}$ means a stronger coupling strength between two ASIRs. The external quality factor $Qex_{1,2}$ and the normalized J-inverter susceptance $J_{1,2}$ can be related by [24] as:

$$Q_{ex1,2} = \frac{\pi}{2\overline{J_{1,2}}^2} \tag{11}$$

The external quality factor $Q_{ex1,2}$ can be further extracted by:

$$Q_{ex1,2} = \frac{f_{c1,2}}{\Delta_{1,2}} = \frac{f_{c1,2}}{\Delta_{(\pm\frac{\pi}{2})1,2}} \tag{12}$$

where, $f_{c1,2}, \Delta_{1,2}, \Delta_{(\pm\frac{\pi}{2})1,2}$ represent the central frequency, -3

dB bandwidths, and the frequency bandwidth of phase curve changing ±π/2 with respect to $f_{c1,2}$, respectively. From (11) and (12), $\overline{J_{1,2}}$ can be calculated by substituting the extracted $Q_{ex1,2}$ into equation (11).

The two transmission lines are represented as two half-wavelength microstrip line resonators. In the filter, the total length (L) of the resonator is equal to $L_1+L_2+L_3+L_4$=32.3mm. So the guided wavelength of the resonator can be calculated as λ_g=64.6mm. Since W/h <1, then the effective dielectric constant can be calculated as:

$$\varepsilon_{re} = \frac{\varepsilon_r+1}{2} + \frac{\varepsilon_r-1}{2}\left\{\left(1+12(W/h)\right)^{-0.5} + 0.04\left(1-(W/h)\right)^2\right\} = 7$$

Then the resonant frequency can be calculated as follows:

$$f_0(GHz) = \frac{300}{\lambda_g(mm)\times\sqrt{\varepsilon_{re}}} = 1.8\ GHz$$

Fig. 5 plots f_0 and external quality factor (Q_{ex1}) versus against L_4 for different gap S_3 values in an SSMCL-ASIR single band type filter. In Fig. 5, when L_4 ranges from 2.7 mm to 8.7 mm, the fundamental frequency f_0 decreases continuously while Q_{ex1} increases in general for a fixed S_3 value. f_0 increases when S_3 ranges from 0.1 mm to 0.4 mm and does not change much when S_3 ranges from 0.4 mm to 0.7 mm, and Q_{ex1} decreases continuously when S_3 ranges from 0.1 mm to 0.7 mm in general. Moreover, it is noted that there are two notches when S_3 = 0.1 mm and 0.7 mm, which means the bandwidth is maximum when L_4 = 5.7 mm within the range of L_4 from 3.7 mm to 8.7 mm.

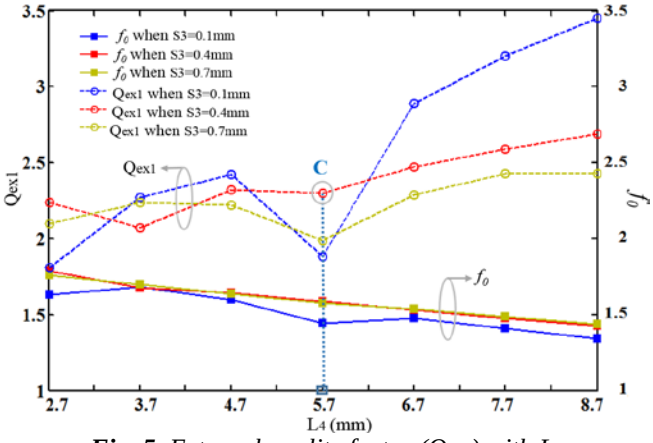

Fig. 5. *External quality factor (Q_{ex1}) with L_4*

By comprehensively considering the bandwidth, resonant frequency location and out-of-band spurious frequency suppression performance, S_3 is set to 0.4 mm, which is shown as point C in Fig. 5.

Fig. 6 plots the variation of coupling bandwidth as a function of the gap size (S_1) between the two resonators. It can be noticed that increasing the gap between the resonators reduces the coupling bandwidth of the designed filer and vice versa. Given the required electrical length ratio α, coupling coefficients and external quality factor for the proposed filter, one may determine the proper specifications based on Figs. 1, 5, 6 and Table 1. The proposed filters, fabricated on an RO3210 substrate with a relative dielectric of 10.2 and dielectric loss tangent 0.003, have been measured using an HP8510 vector network analyser. A wide-band frequency response for the proposed ASIRs is shown in Fig. 7. The simulated S-parameters, measured S-parameters and zoom in-band performance of the designed single-wideband SSMCL-ASIRs are plotted in Fig. 8.

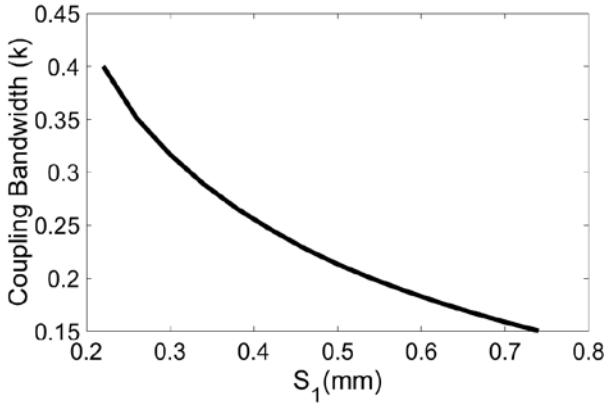

Fig. 6. *Coupling Bandwidth (K) with the gap size (S_1)*

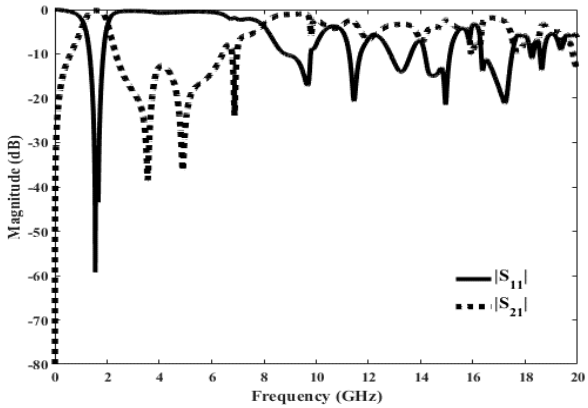

Fig. 7. *Up to 20 GHz frequency response for the proposed ASIRs*

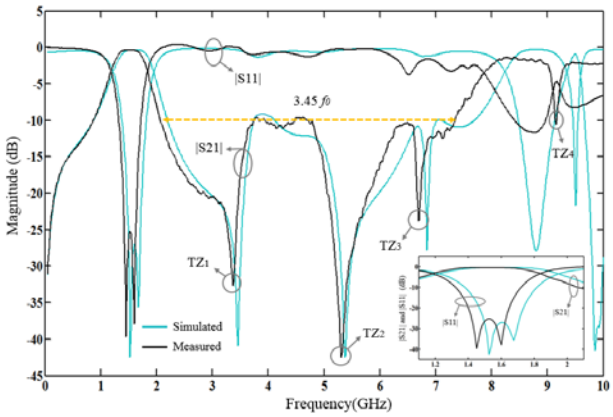

Fig. 8. *Simulated, measured results and zoom in-band performance of single-wideband type SSMCL-ASIRs*

Good agreement can be observed between the simulated and measured results and the slight discrepancies are attributed to loss and fabrication errors. It can be seen that the single-wideband filter is realized with very low insertion isolation of only 0.36 dB at central frequency and return loss of better than 25.5 dB.

The pass band ranges from 1.18-1.84 GHz with central frequency 1.51 GHz, bandwidth 660 MHz and

Table 2 Performance comparison with proposed Single-Band BPF

REF	CF (GHZ)	-3dB FBW	IL (dB)	stop band suppression	number T_{zs}	size	single-/multi-band versatility
[5]	2.4	8.4%	2.06	up to 5.5 f_0	2	$0.36\lambda_g \times 0.13\lambda_g$	no
[9]	1.45	57.9%	1	1.45 f_0-3.35 f_0	4	$0.664\lambda_g \times 0.133\lambda_g$	no
[10]	5	40%	0.7	1.26 f_0-3.52 f_0	2	$0.294\lambda_g \times 0.162\lambda_g$	no
[11]	2.4	--	3.3	3.6 f_0	2	$0.2\lambda_g \times 0.15\lambda_g$	no
This work	**1.51**	**43.7%**	**0.36**	**1.39 f_0-4.85 f_0**	**3**	**$0.063\lambda_g \times 0.50\lambda_g$**	**yes**

fractional band width (FBW) 43.7%. It can be applied in the Global Positioning System (GPS: frequency band centred at 1.57 GHz), Global System for Mobile Communication (GSM: 1800 MHz) and Universal Mobile Telecommunication System (UMTS: 1710-1880 MHz etc.).

Since the adjustable transmission zeros f_{z1} = 3.38 GHz, f_{z2} = 5.31 GHz, f_{z3} = 6.71 GHz are close to the spurious frequencies, a wide stop band ranging from 2.1-7.32 GHz is realized, as shown in Fig. 9(a). Normalized resonant frequencies f_{sj} and transmission zero frequencies f_{zk} locations with the traditional structure are plotted in Fig. 8(a) for comparison. Fig. 9(b) is a photograph of the single-wideband type SSMCL-ASIR, and its performance comparison with others single-band BPFs is shown in Table 2.

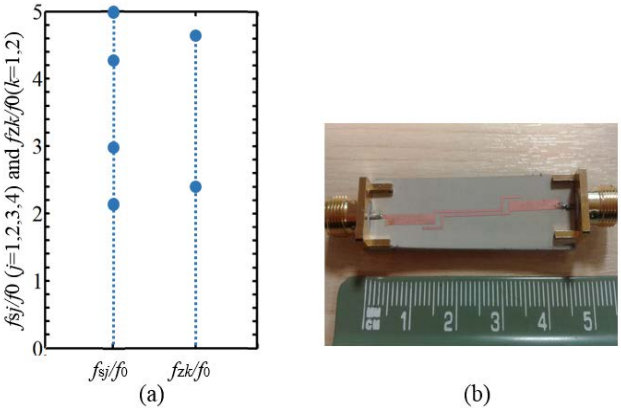

Fig. 9. *(a) f_{sj} and f_{zk} locations of the traditional structure (b) The single-wideband type SSMCL-ASIR filter*

The proposed structure can be extended to higher order modes by cascading the basic building block, i.e. the ASIR resonator. As an example, a three-pole bandpass is shown in Fig. 10 with two TZs on the high side, giving improved out-of-band performance. Higher order filters are obtainable by cascading more building blocks.

4. The Quint-Wideband ASIR Filter Design

As stated above, transmission zeros can be created and utilized to give a multi-band frequency response. The variation of S_{11} and S_{21} for different values of L_4 is shown in Fig. 11. As shown in the figure, because of the multi-path coupling routing and transmission zeros tuning method, six transmission zeros (T_{Z1}-T_{Z6}) are generated, positioned between different pass bands to widen the pass bandwidths and improve the frequency selectivity. Moreover, the fifth operating band of more than 3.5 GHz -3dB bandwidth is generated, which is described as f_{s5} in the figure.

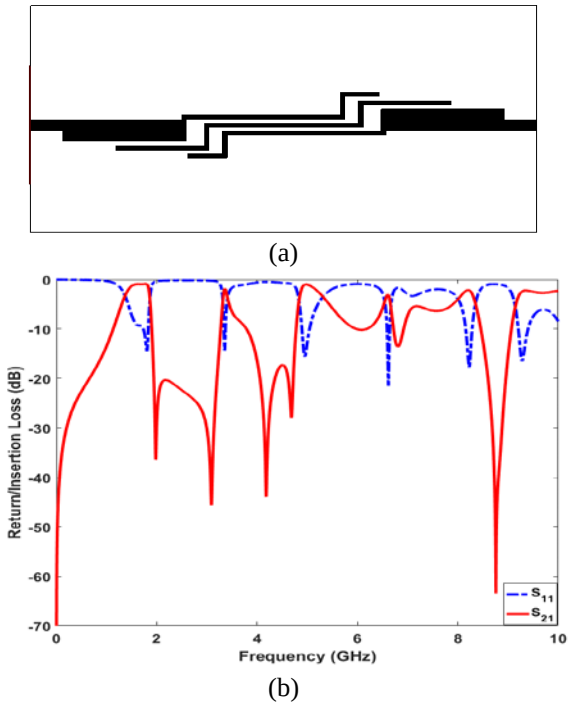

Fig. 10. *(a) Three-pole structure of the proposed filter (b) S-parameter performance for a three-pole structure*

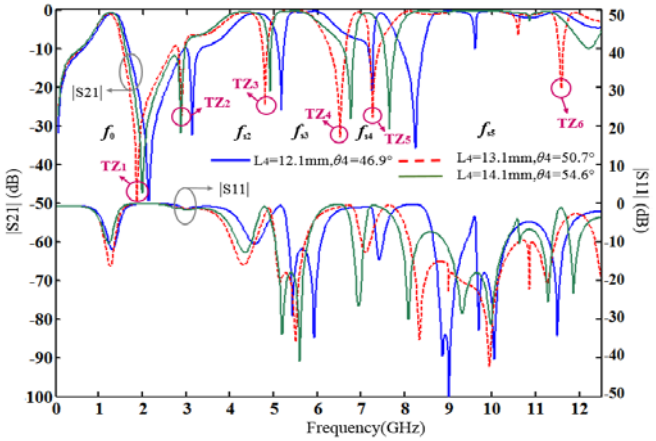

Fig. 11. *Variation of S_{11} and S_{21} versus different values of L_4*

Fig. 12 plots the effect of L_4 on a quint-wideband type SSMCL-ASIR. In (a), when L_4 varies from 10.1 to 16.1 mm, f_0 decreases while Q_{ex1}, normalized f_{s2} and Q_{ex2}/Q_{ex1} fluctuate. In (b), normalized f_{s3}, f_{s4} and f_{s5} increase slightly, and Q_{ex3}/Q_{ex1} fluctuates slightly. In contrast, Q_{ex4}/Q_{ex1} and Q_{ex5}/Q_{ex1} decrease dramatically from 13 to 5.28 and from 7.1 to 1.2, respectively. Moreover, the notch of each Q_{exi}/Q_{ex1} (i = 2, 3, 4, 5) curve happens near L_4 = 13.1 mm, which means

that relatively second, third, fourth and fifth bandwidths of the proposed quint-band filter can obtained with L_4 ~ 13.1 mm.

The design procedures for single- and quint-wideband type SSMCL-ASIR BPFs can be summarized as follows:

1) Choose the suitable electrical length ratio α, thus setting the fundamental frequency f_0, and choose the characteristic impedance ratio K in the ASIR to realize improved insertion loss and return loss performance.
2) Analyse the transmission zero generating requirement of the meander coupled section added to the SS-ASIR structure and calculate the approximate transmission zero equations $S_{21} = 0$.
3) According to the calculated results, tune the length of the meander coupled section to meet $S_{21} = 0$ and make f_{zn} approach the resonant frequency f_{sm} to form a wide stop band for the single-wideband type ASIR filter. The gap parameter S_1 and S_3 are also utilized and tuned to realize optimized results.
4) Tune the length of the meander coupled section to move f_{zn} away from f_{sm}, to enable a multi-band response with good isolation between operating bands for the multi-wideband type ASIR filter.
5) Because of the non-wideband limitation of the coupling matrix, coupling coefficients are not important in this design, while external quality factor Q_{ex} can be discussed for performance optimization, as mentioned above.

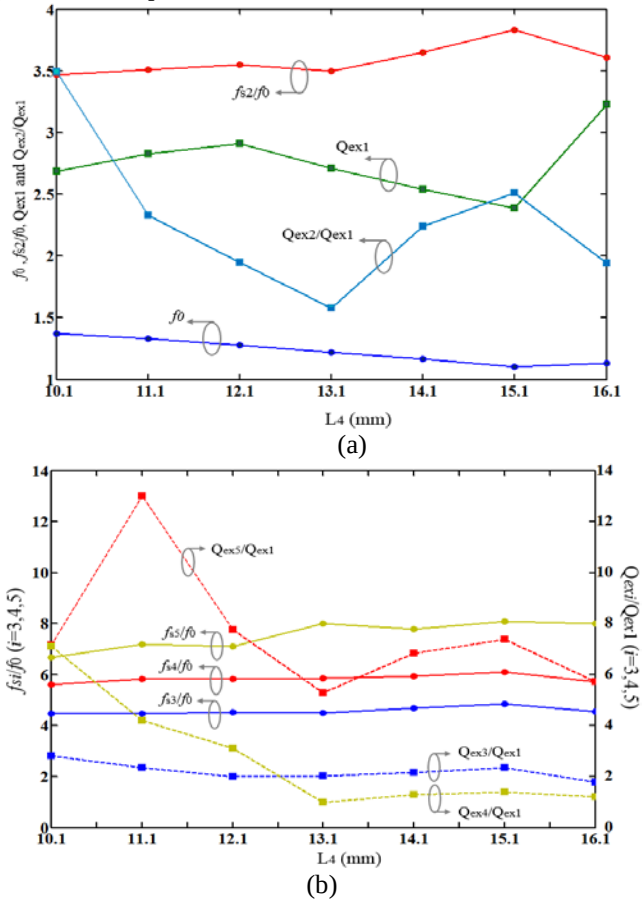

Fig. 12. *The effect of L_4 on quint-wideband type SSMCL-ASIR (a) f_0, Q_{ex1}, $fs2/f_0$ and Q_{ex2}/Q_{ex1} versus against L_4, (b) fsi/f_0 and $Qexi/Qex1$ (i = 3, 4, 5) versus against L_4*

Simulated, measured results and fabricated photograph of the quint-wideband type SSMCL-ASIR filter are plotted in Fig. 13. Good agreement can be observed between the simulated and measured results, with discrepancies attributable to losses and fabrication errors.

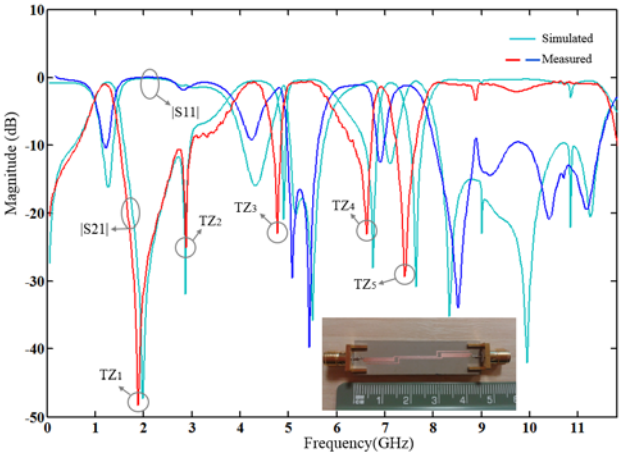

Fig. 13. *Simulated and measured results, and photograph of a modified quint-wideband type SSMCL-ASIR*

It can be seen that quint wide bands are realized with good in-band return loss performance. The first pass band ranges from 1.0 to 1.38 GHz with a central frequency (CF) of 1.19 GHz, and bandwidth (BW) of 380 MHz. The second pass band ranges from 3.96 to 4.62 GHz with CF 4.29 GHz, BW 660 MHz. The third pass band ranges from 5.0 to 5.86 GHz with CF 5.43 GHz and BW 860 MHz. The fourth pass band ranges from 6.82 to 7.12 GHz with CF 6.97 GHz and BW 300 MHz. The fifth pass band ranges from 7.96 to 11.84 GHz with CF 9.9 GHz, and a large BW of 3.88 GHz. In addition, there are five transmission zeros at 1.96 GHz, 2.98 GHz, 4.89 GHz, 6.68 GHz and 7.58 GHz, which further enhance the frequency selectivity, illustrated in Fig. 13. The quint-wideband type SSMCL-ASIR performance comparison with alternative quint-band BPFs is shown in Table 3.

5. Tri-Wideband Band Pass SS-ASIR Filter Design Using Asymmetric Parallel Uncoupled Lines

An uncoupled section placed within conventional coupled lines is a useful way to achieve extra transmission zeros close to existing zeros created by the conventional coupled lines. This way approach can also permit optimization of the in-band performance of the original structure. As indicated in [24], the resonator unit can be further moved horizontally to the left or right so as to provide extra coupling between the coupling resonators. In this paper, the ASIR coupling structure in the vertical direction is further modified and an asymmetric parallel uncoupling microstrip line structure (APUML) is proposed. As shown in Fig. 14 (a), the two ASIR unit impedance line has an extra coupling with the low characteristic impedance line and this coupling length is St.

Moreover, there is a separation distance between two vertical symmetry axes of two parallel uncoupling microstrip lines, and this distance is controlled and influenced by the APUML relative distance parameters L_d, L_{d1} end and parameter S_t. The APUML's height and inner gap are L_m and W_m, respectively. The relative even-mode or odd-mode equivalent circuit of the proposed structure is shown in Fig. 14 (b). Z_{1e} or Z_{1o}, Z_{2e} or Z_{2o} and Z_{3e} or Z_{3o} are respectively the left, middle and right coupled section's even-mode or odd-

Table 3 Performance comparison with proposed Quint-Band BPF

REF	CF(GHZ)	3dB FBW (%)	IL (dB)	size	single-/multi-band versatility	extra structure
[12]	0.6/0.9/1.2/1.5/1.8	5.8/5.2/5.8/8.2/8.0	2.8/2.9/2.9/2.6/2.3	$0.045\lambda_g \times 0.52\lambda_g$	no	via hole
[13]	0.63/1.33/2.03/2.74/ 3.45	28.8/9.4/2.7/5.3/5.5	0.47/1.14/1.8/1.39/ 1.26	$0.043\lambda_g \times 0.178\lambda_g$	no	via hole
[14]	1.5/2.5/3.5/4.5/5.8	4.5/4.5/3.6/4.5/2.7	1.5/1.8/0.9/1.2/ 2.5	$0.24\lambda_g \times 0.17\lambda_g$	no	multi-layer
This Work	**1.19/4.29/5.43/6.97/ 9.9**	**31.9/15.4/15.8/4.3/3 9.2**	**1.0/0.47/0.50/1.7/ 0.6**	$\mathbf{0.05\lambda_g \times 0.40\lambda_g}$	**yes**	**none**

mode impedance. Z_2 and Z_3 or Z_4 and Z_5 are uncoupled sections in two coupled ASIRs, respectively.

Compared to traditional skew-coupled ASIR filters, a wider second pass band is achieved and the additional third operating band is generated by adopting the novel asymmetric parallel uncoupled microstrip lines. It is observed that this greatly improves the coupling strength between the two ASIRs.

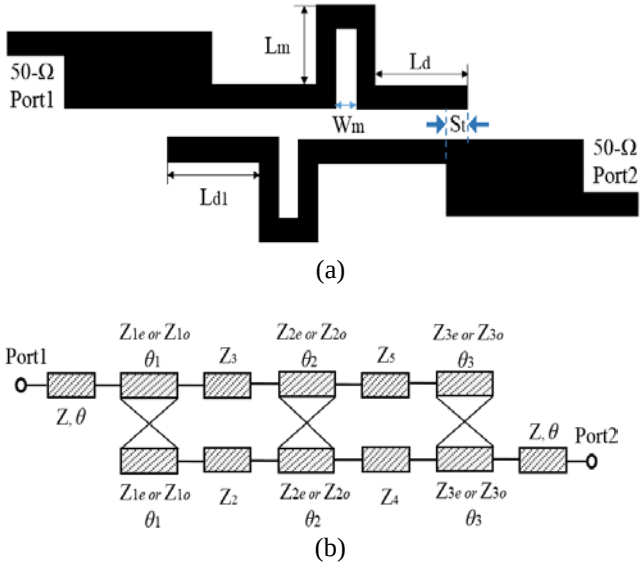

Fig. 14. *The schematic diagram of the SS-ASIR ASIR coupled pair with asymmetric parallel uncoupled meander sections (a) The schematic diagram. (b) Even-mode or odd-mode equivalent circuit*

Fig. 15 illustrates the influence of W_m and L_m on the response of the APUML-ASIR tri-band filter with different values of St. In (a), when Wm varies from 0.05 mm to 0.25 mm, f_0 decreases slightly and f_{s2}/f_0 increases slightly but neither are greatly influenced by varying St. Meanwhile, f_{s2}/f_0 does not change much but does less when St increases. In (b), when Wm varies from 0.05 mm to 0.25 mm, fz1/f0 decreases slightly while f_{z2}, $3/f_0$ hardly changes, but when St becomes greater for a fixed Wm, $f_{z1,2,3}/f_0$ becomes less.

This means transmission zeros can be controlled by Wm and St. In (c), when Lm varies from 1.7 mm to 2.9 mm, $f_{s1,2,3}/f_0$ decreases slightly. When St varies from 1 mm to 4 mm, f_0 and f_{s2}/f_0 do not vary but f_{s1}/f_0 decreases. In (d), when Lm varies from 1.7 mm to 2.9 mm, Q_{ex1} increases and $Q_{ex2,3}/Q_{ex1}$ decreases, so that the fundamental bandwidth becomes narrower. When St becomes greater, Q_{ex1} does not change and $Q_{ex2,3}/Q_{ex1}$ decreases. Compared to f_0, f_{s2}, f_{z1} and f_{z3}, the variation of St has greater influence on the second pass band central frequency f_{s1}, the second transmission zero f_{z2} and the third pass bandwidth.

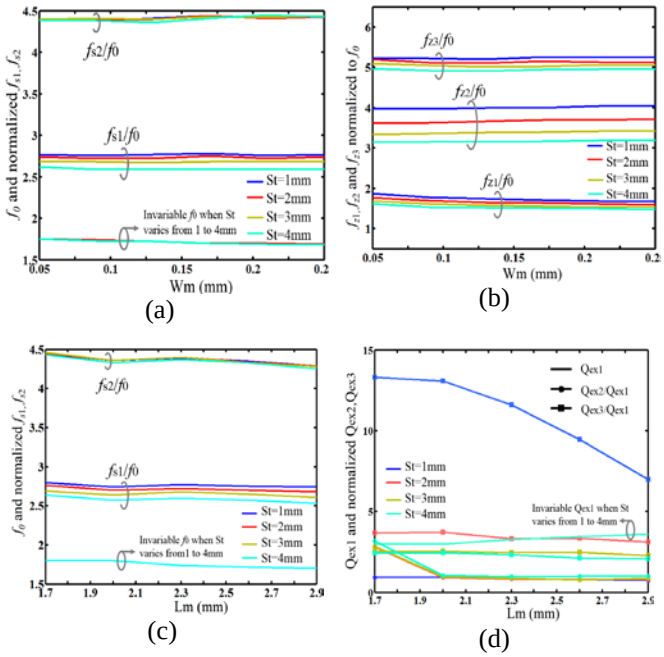

Fig. 15. *The influence of W_m and L_m on the response of the APUML-ASIR Tri-band filter for variation of St: (a) f_0 and normalized f_{si} (W_m varies): (b) Normalized f_{zi}: (c) f_0 and normalized $f_{si,}$ (L_m varies): (d) Q_{ex1} and normalized Q_{exi}. When one parameter varies, the others remain unchanged*

Fig. 16 shows the effect of plots the reference location parameter L_d on the frequency response of the proposed tri-band filter. It is noted that when L_d changes from 5 mm to 7.64 mm when L_{d1} is fixed at 8.1 mm, the second pass band return loss performance is enhanced greatly and its bandwidth becomes wider, providing a wide second pass band of more than 3.5 GHz. At the same time, a third pass band is formed and its return loss as well as its insertion loss performance is improved considerably by varying L_d. Similar phenomenon can be observed when varying L_{d1} with fixed L_d. Therefore, L_d and L_{d1} are two important factors to tune and influence the coupling strength between two modified ASIRs and external quality factors.

The analysis of the asymmetric parallel uncoupled microstrip line unit (APUML) further helps to explain the formation of the second and third pass band. The APUML topological structure and frequency response are plotted in Fig. 17: as seen in the figure, the APUML unit forms two wide pass bands between 4-6 GHz and 6-8 GHz when L_{d1} changes from 9.1 mm to 7.1 mm.

This result proves the advantage of the APUML structure to optimize the in-band filter performance. As for out of band performance, the APUML unit generates four transmission zeros at both sides of the pass bands, as plotted in Fig. 17. These four transmission zeros can improve the isolation performance between the three pass bands, and the out of band suppression performance.

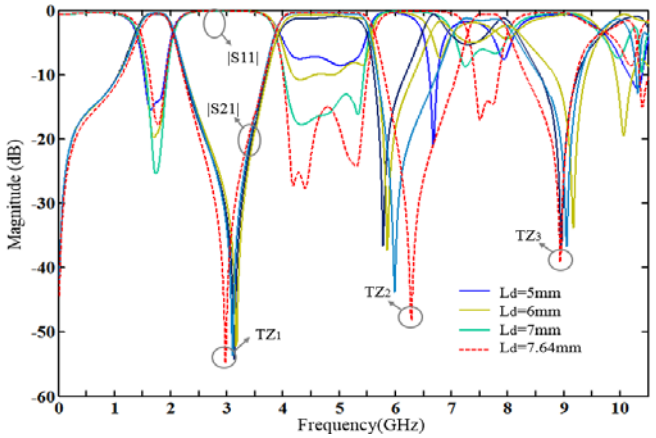

Fig. 16. *The impact of L_d impact on the frequency response of the SS-ASIR filter with APUMLs*

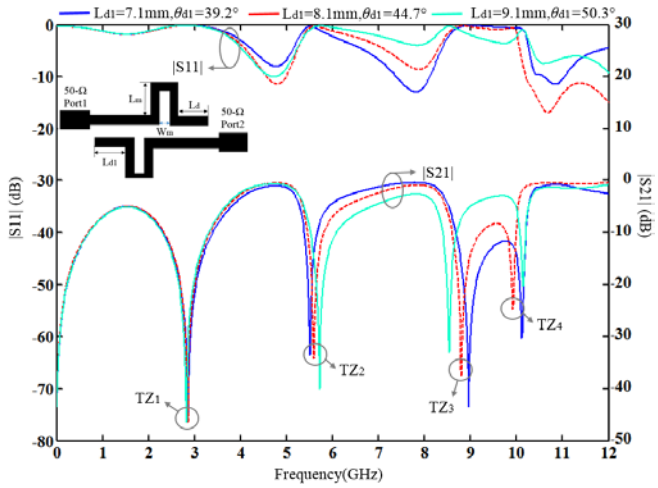

Fig. 17. *The analysis of the APUML structure*

The simulated S-parameters, measured S-parameters and fabricated photograph of the tri-wideband ASIR filter are shown in Fig. 18. Good agreement is observed between the simulated and measured results and the slight discrepancies are attributed to the loss and fabrication errors. It can be seen that triple wide bands are realized with good in-band return loss performance. The first pass band ranges from 1.46-1.98 GHz with a central frequency (CF) of 1.72 GHz, bandwidth (BW) 520 MHz and fractional band width (FBW) 30.2%. It can be applied in the Global Positioning System (GPS: frequency band centred at 1.57 GHz), Global System for Mobile Communication (GSM: 1800MHz) and Universal Mobile Telecommunication System (UMTS: 1710-1880 MHz etc.). The triple-wideband type APUML-ASIR filter performance comparison with alternative tri-band BPFs is shown in Table 4.

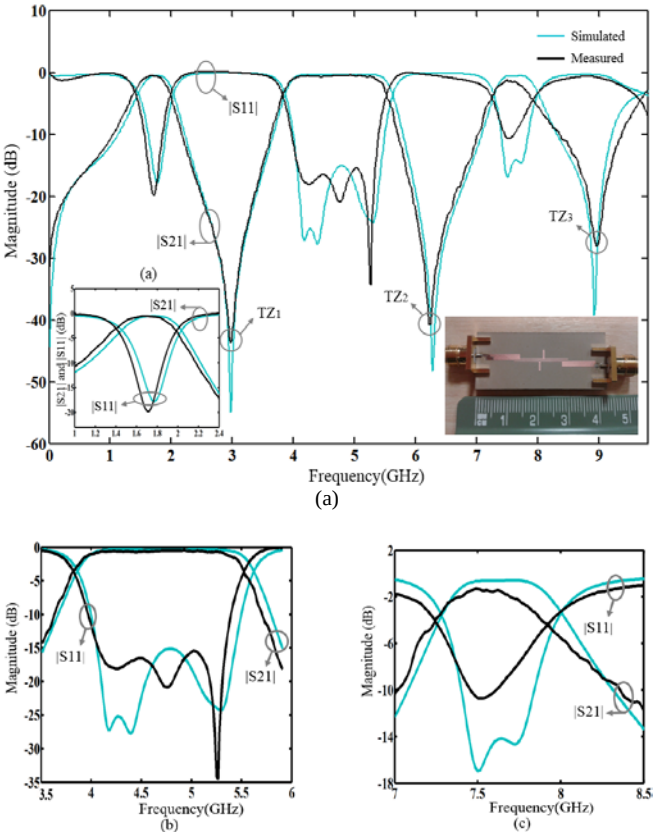

Fig. 18. *Simulated, measured results and fabricated photograph of in SS-ASIRs with APUMLs (a) Narrowband view of the first passband. (b) Narrowband view of the second passband. (c) Narrowband view of the third passband*

Table 4 Performance comparison with proposed Tri-Band ASIR BPF

REF	CF(GHZ)	3dB FBW (%)	IL (dB)	$ISO_{1,2}$, $ISO_{2,3}$	size	extra structure
[13]	1.875/3.54/5.91	19.9/14/4.6	0.6/0.75/1.65	>27 / >20	$0.206\lambda_g \times 0.086\lambda_g$	via hole
[15]	1.8/3.5/5.8	7/5/3.5	0.88/1.33/1.77	>40.4 / >12.78	$0.108\lambda_g \times 0.521\lambda_g$	via hole
[16]	2/3.45/5.8	8.7/13.4/7.2	1.4/0.7/1.7	NA	$0.045\lambda_g \times 0.52\lambda_g$	via hole
[17]	2.4/3.5/5.45	11.6/6.7/17.8	1.1/1.2/1	<40 / <40	$0.21\lambda_g \times 0.11\lambda_g$	via hole
This work	**1.72/4.72/7.59**	**30.2/34.7/7.1**	**0.58/0.43/1.3**	**43.5/39.2**	**$0.09\lambda_g \times 0.51\lambda_g$**	**none**

The second pass band ranges from 3.90-5.54 GHz with CF 4.72 GHz, BW 1.64 GHz and FBW 34.7%. It can be applied in IEEE802.11a WLAN applications including 5G Wi-Fi. The third pass band, which ranges from 7.32-7.86 GHz with CF 7.59 GHz, BW 0.54 GHz and FBW 7.1%, can be applied in earth-satellite satellite communication.
Moreover, good isolation is achieved between the three pass bands, to eliminate signal interference. Three transmission zeros located at 3.02 GHz, 6.26 GHz and 9.01GHz are generated to enhance frequency selectivity, which can be seen in Fig. 18. Furthermore, it is significant that this design can be easily developed to handle and permit reconfigurability [25, 26] and can be easily integrated with antenna design [27], to create the so-called "filtenna" [28].

6. Conclusion

Novel multi-standard single/tri/quint-wideband ASIR filters are proposed in this paper. By utilizing a novel modified SS-ASIR coupled pair with meander coupled sections, and placing transmission zeros close to resonant frequencies, a single-wideband filter with good fractional bandwidth, insertion loss and return loss performance is realized. By varying the lengths of meander coupled sections, stronger coupling between two resonators is realized and more transmission zeros are generated, which are tuned to help in forming a quint operating wideband. With the help of APUML, a tri-wideband ASIR filter is realized with high fractional bandwidth. These filters effectively cover several applications including GPS, GSM, UMTS, ISM and IEEE 802.11 a/b/g/n/ac, with controllable bandwidths. Furthermore, the proposed structures successfully realize ASIR filter applications in single/dual/triple/quadruple/quint-wideband fields with the advantage of higher versatility. Measured results agree well with simulated results and theoretical predictions. The good in-band and out-of-band behavior, compact size and simple structure make the proposed filters very promising for applications in future multi-standard wireless communication.

7. Acknowledgments

This project has received funding from the European Union's Horizon 2020 research and innovation programme under grant agreement H2020-MSCA-ITN-2016 SECRET-722424.

8. References

[1] Lin, S.-C., Deng, P.-H., Lin, Y.-S., Wang, C.-H. and Chen, C. H.: 'Wide-stopband microstrip bandpass filters using dissimilar quarter-wavelength stepped-impedance resonators', *IEEE Trans. Microw. Theory Tech.*, 2006, 54, (3), pp. 1011–1018

[2] Wang, H. and Chu, Q.-X.: 'An EM-coupled triangular open-loop filter with transmission zeros very close to passband', *IEEE Microw. Wireless Compon. Lett.*, 2009, 19, (2), pp. 71–73

[3] Torabi, A. and Forooraghi, K.: 'Miniature harmonic-suppressed microstrip bandpass filter using a triple-mode stub-loaded resonator and spur lines', *IEEE Microw. Wireless Compon. Lett*, 2011, 21, (5), pp.255–257

[4] Kim, C. H. and Chang, K.: 'Wide-Stopband Bandpass Filters Using Asymmetric Stepped-Impedance Resonators', *IEEE Microw. Wireless Compon. Lett.*, 2013, 23, (2), pp. 69-71

[5] Al-Yasir, Y.I.A., Abd-Alhameed, R. A., Noras, J., Abdulkhaleq, A. and Ojaroudi Parchin, N.: 'Design of Very Compact Combline Band-Pass Filter for 5G Applications', Loughborough Antennas & Propagation Conference, 2018, Loughborough, UK

[6] Chen, C.F., Huang, T.Y. and Wu, R.B.: 'Design of microstrip bandpass filters with multiorder spurious-mode suppression', *IEEE Trans. Microw. Theory Tech.*, 2005, 53, (12), pp. 3788-3793

[7] Kuo, T. N., Lin, S. C., Wang, C. H. and Chen, C. H.: 'New Coupling Scheme for Microstrip Bandpass Filters With Quarter-Wavelength Resonators', *IEEE Trans. Microw. Theory Tech.*, 2008, 56, (12), pp. 2930-2935

[8] Xu, J., Ji, Y. X., Miao, C. and Wu, W.: 'Compact Single-/Dual-Wideband BPF Using Stubs Loaded SIR (SsLSIR)', *IEEE Microw. Wireless Compon. Lett.*, 2013, 23, (7), pp. 338-340

[9] Fan, J., Zhan, D., Jin, C. and Luo, J.: 'Wideband microstrip bandpass filter based on quadruple mode ring resonator', *IEEE Microw. Wireless Compon. Lett.*, 2012, 22, (7), pp. 348–350

[10] Luo, X., Ma, J.-G. and Li, E.-P.: 'Wideband bandpass filter with wide stopband using loaded BCMC stub and short-stub', *IEEE Microw. Wireless Compon. Lett.*, 2011, 21, 97), pp. 353–355

[11] Tang, C. W. and You, S. F.: 'Miniaturised wide stopband rejected microstrip filter with coupled spur-lines', *Electronics Letters*, 2006, 42, (5), pp. 286-288

[12] Chen, C. F.: 'Design of a Compact Microstrip Quint-Band Filter Based on the Tri-Mode Stub-Loaded Stepped-Impedance Resonators', *IEEE Microw. Wireless Compon. Lett.*, 2012, 22, (7), pp. 357-359

[13] Xu, J., Wu, W. and Wei, G.: 'Compact Multi-Band Bandpass Filters with Mixed Electric and Magnetic Coupling Using Multiple-Mode Resonator', *IEEE Trans. Microw. Theory Tech.*, 2015, 63, (12), pp. 3909-3919

[14] Hsu, K.W., Hung, W.C. and Tu, W. H.: 'Compact quint-band microstrip bandpass filter using double-layered substrate, *Microwave Symposium Digest (IMS), IEEE MTT-S International*, Seattle, WA, 2013, pp. 1-4

[15] Zhang, S. and Zhu, L.: 'Compact Tri-Band Bandpass Filter Based on λ/4 Resonators With U-Folded Coupled-Line', *IEEE Microw. Wireless Compon. Lett.*, 2013, 23, (5), pp. 258-260

[16] Gao, L., Zhang, X. Y., Hu, B. J. and Xue, Q.: 'Novel Multi-Stub Loaded Resonators and Their Applications to Various Bandpass Filters', *IEEE Trans. Microw. Theory Tech.*, 2014, 62, (5), pp. 1162-1172

[17] Gao, L., Zhang, X.Y. and Xue, Q.: 'Compact Tri-Band Bandpass Filter Using Novel Eight-Mode Resonator for 5G WiFi Application', *IEEE Microw. Wireless Compon. Lett.*, 2015, 25, (10), pp. 660-662

[18] Kim, C. H. and Chang, K.: Independently Controllable Dual-Band Bandpass Filters Using Asymmetric Stepped-Impedance Resonators', *IEEE Trans. Microw. Theory Tech.*, 2011, 59, (12), pp. 3037-3047

[19] Chang, Y. C., Kao, C. H., Weng, M. H. and Yang, R. Y.: 'Design of the Compact Wideband Bandpass Filter with Low Loss, High Selectivity and Wide Stopband', *IEEE Microw. Wireless Compon. Lett.*, 2008, 18, (12), pp.770-772

[20] Kim C. H. and Chang, K.: Wide-Stopband Bandpass Filters Using Asymmetric Stepped-Impedance Resonators', *IEEE Microw. Wireless Compon. Lett.*, 2013, 23, (2), pp. 69-71

[21] Liu, H. W.: 'High-Temperature Superconducting Bandpass Filter Using Asymmetric Stepped-Impedance Resonators With Wide-Stopband Performance', *IEEE Trans. Applied Superconductivity*, 2015, 25, (5), pp. 1-6

[22] Wu, H. W. and Yang, R. Y.: 'A New Quad-Band Bandpass Filter Using Asymmetric Stepped Impedance Resonators', *IEEE Microw. Wireless Compon. Lett.*, 2011, 21, (4), pp. 203-205

[23] Hong, J. S. and Lancaster, M. J.: 'Microstrip Filter for RF/Microwave Applications' (Wiley, 2001)

[24] Azadegan, R. and Sarabandi, K.: 'Miniature high-Q double-spiral slot-line resonator filters', *IEEE Trans. Microw. Theory Techn.*, 2004, 52, (5), pp. 1548-1557

[25] Yuceer, m.: 'A reconfigurable microwave combline filter', *IEEE Transactions on Circuits and Systems II, Express Briefs*, 2016, 63, (1), pp. 84–88

[26] Al-Yasir, Y. I. A, Ojaroudi Parchin, N., Abd-Alhameed, R., Abdulkhaleq, A. and Noras, J. 'Recent Progress in the Design of 4G/5G Reconfigurable Filters" *Electronics*, 2019, 8, (1), pp. 1-17

[27] Al-Yasir, Y. I. A, Abdullah, A, Mohammed, H, Abd-Alhameed, R. and Noras, J:: 'Design of Frequency-reconfigurable Multiband Compact Antenna using two PIN diodes for WLAN/WiMAX Applications', *IET Microwaves, Antennas and Propagation*, 2017, 11, (8), pp. 1098-1105

[28] Atallah, H., Abdul Rahman, A., Yoshitomi, K. and Pokhare, P.: 'Compact frequency reconfigurable filtennas using varactor loaded t-shaped and h-shaped resonators for cognitive radio applications', *IET Microwaves, Antennas and Propagation*, 2016, 10, (9), pp. 991–1001